Environ. Sci. Technol. 1992, 26, 1752–1759

(4) Szetela, R. W.; Winnicki, T. Z. *Biotechnol. Bioeng.* **1981**, *23*, 1485.
(5) Sokol, W. *Biotechnol. Bioeng.* **1988**, *32*, 1097.
(6) Beltrame, P.; Beltrame, P. L.; Carniti, P.; Pieta, D. *Water Res.* **1979**, *13*, 1305.
(7) Rozich, A. F.; Gaudy, A. F., Jr.; D'Adamo, P. D. *Water Res.* **1983**, *17*, 1453.
(8) Rozich, A. F.; Gaudy, A. F., Jr.; D'Adamo, P. C. *Water Res.* **1985**, *19*, 481.
(9) Rozich, A. F.; Gaudy, A. F., Jr. *J. Environ. Eng.* **1984**, *110*, 562.
(10) Rozich, A. F.; Gaudy, A. F., Jr. *J.—Water Pollut. Control Fed.* **1985**, *57*, 795.
(11) Uzman, S.; Yongacoglu, S.; Walker, B.; Dunn, I. J. Dynamics of Phenol and Oxygen Uptake in a Biological Wastewater Treatment Reactor. In *Treatment and Disposal of Liquid and Solid Industrial Wastes*; Curi, K., Ed.; Pergamon Press: New York, 1980; pp 73–87.
(12) Pawlowsky, U.; Howell, J. A.; Chi, C. T. *Biotechnol. Bioeng.* **1973**, *15*, 905.
(13) Andrews, J. F. *Biotechnol. Bioeng.* **1968**, *10*, 707.
(14) Radhakrishnan, I.; Sinha Ray, A. K. *J.—Water Pollut. Control Fed.* **1974**, *46*, 2393.
(15) Chi, C. T.; Howell, J. A. *Biotechnol. Bioeng.* **1973**, *15*, 905.
(16) Yang, R. D.; Humphrey, A. E. *Biotechnol. Bioeng.* **1975**, *17*, 1211.
(17) Okaygun, M. S. Ph.D. Dissertation, Texas A&M University, 1991.
(18) Marquardt, D. M. *J. Soc. Ind. Appl. Math.* **1963**, *11*, 431.

Received for review November 14, 1991. Revised manuscript received May 4, 1992. Accepted May 6, 1992. This project was funded through 041TAM 0203 from the Gulf Coast Hazardous Substance Research Center. Their contribution is greatly appreciated.

Field Study and Numerical Simulation of Subslab Ventilation Systems

Yves C. Bonnefous,† Ashok J. Gadgil,*,† William J. Fisk,† Richard J. Prill,‡ and Albert R. Nematollahi†

Indoor Environment Program, Lawrence Berkeley Laboratory, 90-3058, 1 Cyclotron Road, Berkeley, California 94720, and Washington State Energy Office, Washington Energy Extension Service, 1212 North Washington Street, Suite 106, Spokane, Washington 99201-2401

■ The effectiveness of the technique of subslab ventilation (SSV) for limiting radon entry into basements was investigated through complementary experimentation and numerical modeling. Subslab pressure fields resulting from SSV were measured in six well-characterized basements, each with a different combination of soil and aggregate permeability. The relationship between air velocity and pressure gradient was measured in the laboratory for the three types of aggregate installed beneath the basement slabs. A new numerical model of SSV was developed and verified with the field data. This model simulates non-Darcy flow in the aggregate. We demonstrate that non-Darcy effects significantly impact SSV performance. Field data and numerical simulations indicate that increasing the aggregate permeability within the investigated range of 2×10^{-8}–3×10^{-7} m^2 substantially improves the extension of the subslab pressure field due to SSV operation. Sealing of cracks in the slab and excavation of a small pit where the SSV pipe penetrates the slab also dramatically improve this pressure field extension. Our findings are consistent with the results of prior field studies; however, the studies reported here have improved our understanding of factors affecting SSV performance. The dependence of SSV performance on the relevant parameters are currently under investigation with the model.

Background

Within the United States, exposure to the radioactive decay products of radon (^{222}Rn) in buildings is the most important source of human exposure to environmental radiation and also one of the largest sources of risk to human health caused by an indoor pollutant (*1*). In houses with elevated indoor Rn concentrations, the primary source of Rn is usually the surrounding soil where Rn is generated by the radioactive decay of trace amounts of radium. The predominant process of Rn entry into houses with a concrete basement is pressure-driven flow of high-Rn soil gas into the basement through small cracks, joints, and holes in its concrete envelope (*2*).

Subslab ventilation (SSV) is one of the most effective and common methods of reducing indoor Rn concentrations in houses with basements. There are two basic methods of SSV. In subslab depressurization (SSD), a fan exhausts soil gas from beneath the slab floor to the outside. The fan usually draws air through one or more plastic pipes that penetrate the slab floor. This process decreases the pressure beneath the floor and, therefore, reverses the pressure difference that normally causes soil gas and Rn to flow into the structure. In subslab pressurization (SSP), outdoor air is forced beneath the slab using a fan (i.e., the direction of air flow is reversed compared to that in a SSD system). SSP ventilates the soil beneath the slab floor, thus reducing radon concentrations within the soil near the slab. Soil gas entry into the structure continues, but the concentration of Rn in the entering soil gas is decreased.

SSV has become a widely used Rn control measure. During construction of new houses, provisions that increase the effectiveness or ease the installation of SSV systems are sometimes recommended or required by code (*3–5*). The most common provision is a layer of highly permeable (clean and coarse) aggregate beneath the slab floor. Based primarily on our general understanding of flow through permeable media and informal evidence from field studies of SSV, a high-permeability aggregate layer improves the extension of the pressure field beneath the slab caused by SSV operation (i.e., the high-permeability aggregate results in a smaller pressure loss with distance from the point of air withdrawal or supply).

In short-term experimental assessment of SSD system performance, prevention of convective radon entry from subslab regions into the basement can be assured if the depressurization imposed at the pit decreases the pressure throughout the subslab region to values below the pressure in the basement, just above the slab. This is a crucial point because a main entry path for radon-bearing soil gas is the crack that commonly occurs at the wall/footer/slab joints, i.e., at the basement periphery; see Figure 1. This reversal of the pressure difference that normally drives radon-bearing soil gas into the basement, at all possible points of entry, stops convective entry of radon.

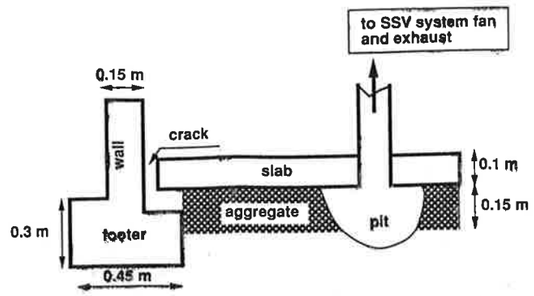

Figure 1. Vertical cross section of a portion of a basement and its surroundings. The crack at the wall/footer/slab joint is shown greatly exaggerated. The dimensions are typical ones. Typical crack width ranges from 0.5 to 3 mm.

Claims of improved SSV performance due to the presence of continuous subslab aggregate layers (compared to no aggregate) are rarely debated. For example, Furman and Hintenlang (*6*) showed that a layer of aggregate located above sand clearly improves pressure field extension beneath test slabs. However, the impact of aggregate type (e.g., permeability) on SSV performance is controversial and is also the primary focus of this paper. Some relevant information has been previously published. Matthews et al. (*7*) presented a closed-form model for cylindrical flow in a subslab aggregate layer (flow through the soil or through cracks in the slab are neglected). They used experimental data on pressure field extension to determine the value of constants within the model and reported a good correlation between measurements and predictions. The final model indicates that air velocity within the aggregate (during their experiments) is approximately proportional to the pressure gradient raised to the 0.7 power and that pressure field extension will improve with increased aggregate permeability. In 1989, Barber (*8*) presented a numerical model of SSV in Florida-style slab on grade housing with sand (but not aggregate) located beneath the slab. As shown later, a model of Darcy flow is not adequate for simulations of SSV performance when an aggregate layer is located beneath the slab.

A recently published paper by Gadsby et al. (*9*) focused specifically on SSV performance as a function of aggregate type. In the laboratory, they studied air velocity (V) versus pressure gradient (dP/dx) in four different types of aggregate. They did not assume Darcy flow; instead they employed the exponential form of non-Darcy flow. The experimental data are used in a closed-form model that approximately emulates the condition of aggregate located between a basement floor and soil. The assumed geometry is a cylindrical layer of aggregate surrounded by a cylindrical annulus of soil (which represents the soil adjacent to the basement walls), bounded from both above and below by two impermeable circular disks. Flow occurs in the radial direction toward a central suction point. The major limitations of this model, other than the simplified geometry, are as follows: (a) flow through cracks in the slab and through the soil beneath the aggregate is neglected; (b) eq 1 of their paper (*9*) is dimensionally incorrect; and (c) the simplifications in the model are inappropriate for very high soil permeabilities (close to aggregate permeabilities) because the flow through the soil beneath the aggregate cannot then be neglected. On the basis of this model and the measured aggregate data, the authors of ref 9 concluded that pressure field extension is more dependent on soil permeability than aggregate permeability.

The research described in the subsequent sections of this paper represents an additional advance in both experimental assessment and numerical modeling of SSV performance.

Objectives and Approach

The primary objective of this research was to determine quantitatively the influence of subslab aggregate type on the performance of SSV systems. Secondary objectives were the development of a more complete model of SSV and to investigate SSV performance as a function of selected SSV system parameters, building substructure, and soil characteristics (e.g., the magnitude of the depressurization at the suction point, the size and location of cracks in the slab, and the permeability of the soil). This paper describes the first part of this research effort; parametric studies are currently underway.

The research approach involves coordinated field experiments in new houses located in the Spokane, WA, area; laboratory characterization of flow through aggregate samples obtained from these house sites; and numerical modeling.

Field Experiments. Six houses with basements were identified during their planning stage for field experiments. The criteria for site and house selection were relatively homogeneous soil, level or simply sloping ground surface, large variability in soil permeability between sites, and a relatively simple basement geometry. The houses were built with one of three types of aggregate beneath the slab floor; thus, each house represented a unique combination of soil permeability and aggregate type. Relevant details for SSV system performance, including the size and location of footings and the depth of the aggregate layer (approximately 10 cm) as a function of position, were monitored and documented during house construction.

Soil permeability was measured using a previously described in situ technique (*10*), generally at two locations within the backfill 0.2 m from the basement walls, two locations within the undisturbed soil approximately 3 m from the basement walls, and two locations 1.3 m beneath the aggregate layer.

Experiments were conducted at each house to assess pressure field extension beneath each slab. All visible large cracks and holes in the slab, except the typical gap (wall/slab gap) at the junction of slab and basement walls, were sealed. Temporary SSV systems were installed and operated at each house while measuring the flow rate in the SSV system, the pressure where the SSV pipe penetrated the slab, the pressure at 3 or 4 locations in the backfill area, and the difference between subslab and above-slab pressure at 22–35 locations (depending on the house geometry).

Several experiments were undertaken in most houses. Parameters or operating conditions that varied between experiments include (a) the choice of SSD or SSP, (b) the magnitude of the pressure at the suction or pressurization point (where the SSV pipe penetrates the slab), (c) the presence or absence of a 25-cm radius hemispheric open pit beneath the slab at the suction or pressurization point (called the SSV pit), and (d) open or sealed perimeter wall/floor crack.

Aggregate Characterization. The aggregates were obtained from local suppliers. The most permeable aggregate type, called $1^1/_2$-in. round or $1^3/_4$-in. round by the supplier, is approximately equivalent to ASTM grade no.

† Lawrence Berkeley Laboratory.
‡ Washington Energy Extension Service.

0013-936X/92/0926-1752$03.00/0

4 (ASTM 1984). The medium permeability aggregate, called $^3/_4$-in. round by the supplier, is approximately equivalent to ASTM grade no. 67. The lowest permeability aggregate, called $^3/_8$-in. exposed or no. 8 pea gravel, is approximately equivalent to ASTM grade no. 8. Standard information on particle size distribution (i.e., fraction that passes through various size screens) was obtained from the suppliers.

Samples of the aggregate beneath each slab were shipped to the Lawrence Berkeley Laboratory (LBL). The relationship between velocity and pressure drop in one sample of each type of aggregate was measured in the laboratory. The basic procedure was to fill a section (25.4 cm by 22.2 cm by 244.0 cm) of a nearly airtight box with aggregate, to force air through the aggregate at different rates, and to measure the pressure difference between two locations, one immediately upstream and the other immediately downstream of the aggregate bed. In the experiments conducted with the highest permeability aggregate, helium was used in place of air during some tests so that pressure differences could be accurately measured during tests when Darcy flow is expected (i.e., tests with low characteristic Reynolds numbers). The laboratory data were analyzed to determine the permeability of the aggregate samples and the value of another flow-related parameter called the Forchheimer factor (defined subsequently). More information on the aggregate samples and the methods and results of laboratory experiments is provided in Gadgil et al. (*11*).

Modeling. A few sophisticated numerical models have been recently developed to compute the generation and the transport of radon in the soil and its entry into a basement (*12–14*). However, they all assume Darcy's law to determine the soil gas velocity as a function of pressure gradient in the soil.

Loureiro and others use a finite difference method in three-dimensional Cartesian coordinates to model the house and the soil block (*12*). Pressure and velocity fields are calculated by solving the Laplace equation resulting from the combination of Darcy's law and the continuity equation with the Boussinesq approximation. Darcy's law is a valid description of soil gas (and radon transport) driven by the natural depressurization of a house (about 5 Pa). However, it is not a valid description of SSV operation because of the high velocities of soil gas occurring in the subslab aggregate (up to 1 m/s). At high velocities, inertial losses, which are proportional to the velocity squared, cannot be neglected. Substantial changes in the algorithms and the solution procedure are necessary to describe non-Darcy flow, compared to the Darcy flow models. Therefore, a new three-dimensional non-Darcy flow simulation model called non-Darcy simulation of transport of air and radon (non-Darcy STAR) was developed to simulate SSV system performance.

The newly developed model solves the *Darcy–Forchheimer* expression of non-Darcy flow (*15*), eq 1, together with the continuity equation (assuming incompressible gas), eq 2

$$\vec{\nabla}p = -(\mu/k)(1 + c|\vec{V}|)\vec{V} \quad (1)$$

$$\vec{\nabla}\cdot\vec{V} = 0 \quad (2)$$

where p is the disturbance pressure (i.e., pressure change due to the depressurized basement and/or operation of a SSV system), $\vec{V}$ is the gas velocity, k is the permeability of the porous media, μ is the dynamic viscosity of the fluid, and c is the Forchheimer term.

Notice that the two equations can no longer be easily combined, and the methods used for solving the Laplace equation, for Darcy flow, are no longer applicable to solve the system of equations.

Once the velocity and pressure fields for the soil gas are determined, the radon concentration field in the soil and the radon entry rate could be computed by separately solving the radon mass balance, as done by Revzan et al. (*14*).

The solution procedures use a finite difference method, using primitive variables (i.e., fluid pressure and velocity components rather than three-dimensional versions of vorticities and stream function) and staggered grids for the pressure and the velocity components. We use the alternate direction implicit (ADI) method of iterative solutions. Computations are carried out by using dimensionless variables. The overall computational approach is similar to that described by Patankar (*16*). The grid generation is done by a nonautomated or "by-hand" description of the real house. This provides ample accuracy in the solution but also implies less flexibility in changing the grid scheme rapidly to other house geometries. In general, for each house, we modeled a soil block of about 27 × 27 m in area centered on the house, and 12.5 m deep below the soil surface. Detailed description of house and soil block geometry used in the model is given in Gadgil et al. (*11*).

The model presently incorporates the following three assumptions, each of which can be relaxed: (a) each material (i.e., soil, backfill, and aggregate) is homogeneous and isotropic; (b) the concrete is perfectly impermeable except for cracks; and (c) the effect of buoyancy on the soil-gas flow field is negligible.

The solution procedure employs an iterative approach to convergence. Iterations are stopped when the maximum residual in the pressure field (defined as the fractional change in pressure at any given node from one iteration to the next) falls below 10^{-6}. Computational requirements increase very rapidly with increasing grid density (i.e., the number of nodes in the computational domain). Therefore, avoiding demands on computational resources must be balanced against retaining an acceptable accuracy of the numerical solutions. Preliminary studies of sensitivity of predictions to the grid density were conducted with a two-dimensional version of the program. For the simulations reported in this paper, we selected a grid layout and a density that provided results for pressure field values within 20% of the values obtained with a finer grid that has eight times as many nodes.

Model Verification

The numerical model was verified by simulating field experiments performed on selected houses in the Pacific Northwest and comparing simulation predictions with experimental results. Verification of the model was considered successful if the predicted soil-gas flow rate through the SSV suction pipe agreed with the measured value and the predicted subslab pressures at various points in the basement agreed with those measured experimentally, within experimental uncertainties, and uncertainties in the model input data. Four tests at house 002 and two tests at house 003 were simulated. The permeabilities and Forchheimer factors for the subslab aggregates measured in the laboratory, the permeabilities of the soil and backfill material measured in situ, the applied pressure at the SSV pit measured during the tests, and the geometrical description of the houses were used as inputs to the simulations. The simulations assumed no pressure difference between the basement and the outside during the tests because the basements (and the houses) were unheated and open to the outside during field experiments. The cracks between the basement slab and the wall/footers

Table I. Permeabilities (k), Forchheimer Terms (c), and Crack Widths for Modeling of Houses 002 and 003

	aggregate	soil	backfill	crack, mm
house 002	$k = 3 \times 10^{-7}$ m^2	$k = 10^{-10}$ m^2	$k = 10^{-10}$ m^2	1.1 L-shaped
	$c = 20$ s/m	$c = 0$ s/m	$c = 0$ s/m	
house 003	$k = 2 \times 10^{-8}$ m^2	$k = 10^{-11}$ m^2	$k = 10^{-11}$ m^2	0.75 L-shaped
	$c = 6$ s/m	$c = 0$ s/m	$c = 0$ s/m	

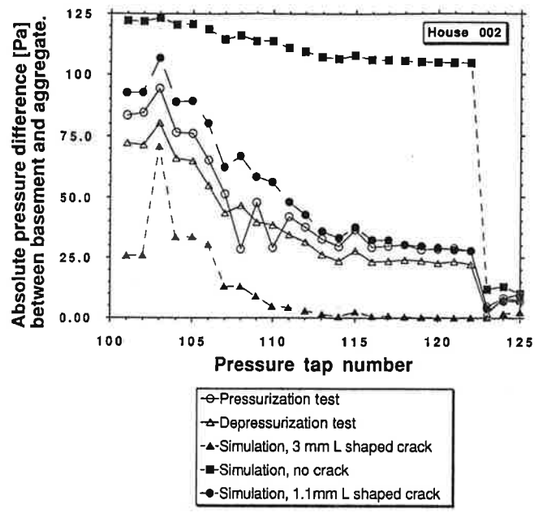

Figure 2. Comparison of field measurements and numerical predictions of subslab pressures at various points in house 002.

were assumed to be of uniform thickness at all wall/footer/slab joints (i.e., at the basement periphery and around the central footer). The input parameter values for these simulations are shown in Table I.

The average or effective thickness of the cracks cannot be measured experimentally in a reliable manner. We show (Figure 2) the predictions from two simulations for house 002 with a 125-Pa depressurization at the SSV pit, one simulation with perfectly sealed cracks and another with wide (3-mm) L-shaped cracks. The predictions bracket the experimental data for subslab and backfill pressures at all the points. Furthermore, we also show in Figure 2 that prediction, made by assuming a 1.1 mm wide L-shaped crack along all the slab-footer joint, agreed well with experimental data for pressures collected at 22 different subslab locations and 3 points in the backfill region. The locations of the measurement (and prediction) points for subslab and backfill pressures are shown in Figure 3 on a schematic floor plan of house 002. The measured flow during field experiments and the predicted flow in the SSV pipe also agreed well (within 10%). Figure 2 also provides data from two tests which have respectively SSD and SSP operation with a suction (or pressure) of 125 Pa applied at the SSV pit.

Two additional tests at house 002 (SSD and SSP operation using 200 Pa) were then simulated without changing any of the other input parameters in the model. The predictions again agreed well with the experimental pressure data at the measurements points (comparison not shown for brevity).

A similar verification exercise was undertaken for house 003. The measured pressures are reasonably well matched by predictions assuming a 0.75-mm L-shaped crack at all

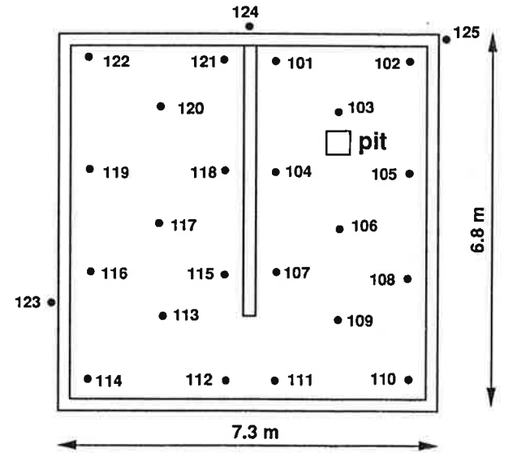

Note: Not to scale

Figure 3. Subslab pressure tap locations and identification numbers in the basement slab of house 002. Perimeter, interior footings, and the location of the SSV pit are shown.

Figure 4. Comparison of field measurements and numerical predictions of subslab pressures at various points in house 003.

slab/footer joints (see Figures 4 and 5).

Discussion. It should be noted that while the sets of input parameters shown in Table I are certainly realistic and consistent with measurement data on soil and aggregate permeability values, there exist enough uncertainties in the experimental data on these values that the input parameter set is not unique. For example, choice of a somewhat higher permeability for the soil and a narrower crack thickness leads to similar predictions from the simulations. We can also obtain further improvements in the agreement with experimental data by assuming nonuniform crack thickness along the slab/footer joints and inhomogeneous soil permeability. However, in the absence of experimental evidence in support of such artifacts in the input data to the simulations, the excellent agreement of resulting simulation predictions with experimental measurements becomes a mere curiosity. The agreement between simulation predictions and field experimental data shown in Figures 2 and 4 is therefore considered adequate under these circumstances.

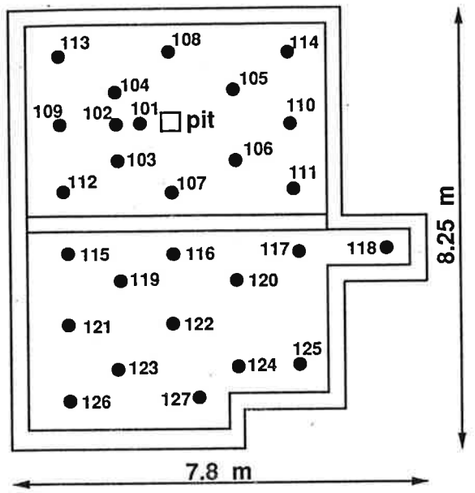

Note: not to scale

Figure 5. Subslab pressure tap locations and identification numbers in the basement slab of house 003. Perimeter, interior footings, and the location of the SSV pit are shown.

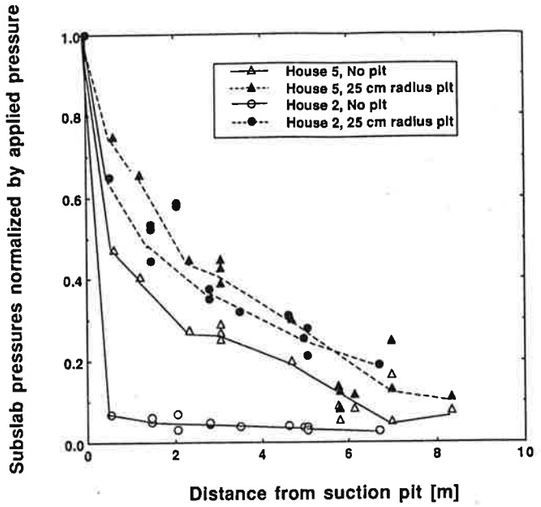

Figure 6. Effect of pit in the subslab gravel at the point of SSV installation. Subslab pressure field extension for houses 002 and 005 improved substantially after a 25-cm radius pit was excavated in the subslab gravel at the point of SSV installation. The lines on these figures connect data from the same subsets of the measurement locations and are intended only for visual guidance.

To assess the importance of modeling non-Darcy flow, we set the Forchheimer term to zero (so eq 1 becomes Darcy's law) in the soil, backfill, and aggregate and reran the simulation for house 002 with −125-Pa depressurization at the pit and a 1.1-mm L-shaped crack. The predicted subslab pressures for the Darcy flow simulation were larger by 12–88% than the non-Darcy flow simulation predictions. To match the Darcy flow predictions with the experimental pressure field values, we had to increase the crack size to 2 mm. While this resulted in an appropriate match between predicted and measured pressure fields, the predicted SSV flow became 4 times larger than its experimentally measured value. We conclude that a Darcy model cannot match both measured pressures and flow rates. Lastly, local Reynolds numbers (based on gravel diameter), *Re*, computed from the Darcy simulation exceed 10 000 in the gravel near the cracks, while the upper limit of *Re* for applicability of Darcy flow is in the range 0.1–75 (*17*). This emphasizes the need for a non-Darcy flow model to simulate SSV systems.

Trends in Field Data and Simulation Predictions

This section describes the dependence of subslab pressure fields on selected features of the SSV system and substructure and also on the ratio of aggregate to soil permeability. The trends are based on field data, and in most cases, the same dependence is illustrated with numerical predictions. The qualitative correspondence of the trends in the experimental results and numerical predictions serves as an additional confirmation of model performance.

Effect of a Pit. Field data demonstrate that excavating a small (25-cm radius) pit at the point of SSV system penetration through the slab substantially improves the extension of the pressure field in the subslab region (see Figure 6, where measured pressure differences at test holes have been normalized by depressurization at the pit). This beneficial effect of a SSV pit has also been demonstrated in prior research (*6*). In the absence of a pit, the extension of the pressure field can be expected to be affected by the specific details of the arrangement of the aggregate particles immediately adjacent to the hole in the slab. In addition, the aggregate could be plugged with concrete at the location of the hole in the slab. Since SSV system performance is more reliable and effective when the SSV systems are installed with a pit excavated in the subslab aggregate, all further investigations on the effectiveness of SSV system performance assume that the SSV system installations have already incorporated this basic and inexpensive measure; we explore effects of other factors on SSV performance.

Effect of the Magnitude of Applied Pressure. Experimental data for house 002 show that the average of the decrease in the normalized pressures (range 0–1) at all subslab points is 15% when the depressurization at the suction pit, P_{pit}, is changed from −125 to −200 Pa. Numerical predictions show a similar but somewhat smaller decrease of 7%. Figure 7 illustrates this effect for the points located in the same bay as the suction pit. The trend is due to non-Darcy flow of soil gas during SSV operation; at larger depressurizations, there is a larger departure from Darcy law. At larger values of P_{pit}, soil-gas velocities in the aggregate increase, and as noted previously, inertial losses increase in proportion to the velocity squared.

Effect of the Ratio of Aggregate Permeability to Soil Permeability. From analogy with electrical circuit theory, the subslab aggregate should yield excellent subslab pressure field extension (i.e., act approximately as a uniform pressure manifold), if the ratio of aggregate permeability to soil permeability is large. Conversely, as this ratio decreases toward unity, the pressure field extension in the subslab region should get progressively poorer because the resistance to soil-gas flow through the aggregate is no longer significantly less than the resistance to flow through the soil beneath the aggregate.

Experimental confirmation of this effect is shown in Figure 8a, using data from three different houses. Since each house has a somewhat different geometry, these data are not directly intercomparable. For Figure 8a, the terms loose soil and tight soil refer respectively to soil permeabilities greater than 10^{-11} m^2 and smaller than 10^{-13} m^2. For Figure 8a,b, the permeabilities of the different gravels are tight gravel, $k = 2 \times 10^{-8}$ m^2; medium gravel, $k = 10^{-7}$ m^2; and loose gravel, $k = 3 \times 10^{-7}$ m^2. Simulations with *non-Darcy STAR* of SSV operation for house 002 geometry and loose soil ($k = 10^{-10}$ m^2) and using different aggregate permeabilities also indicate that the ratio of aggregate permeability to soil permeability has a critical impact on the subslab pressure field extension (see Figure 8b). Generalization of this effect, in terms of its expression as a single equation, is under investigation.

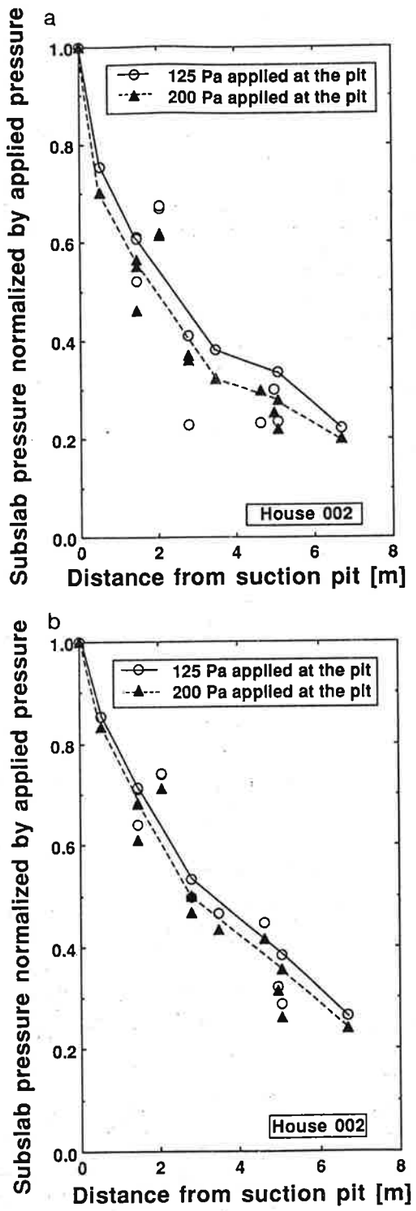

Figure 7. Non-Darcy flow lowering the normalized subslab pressure at all points: (a) when P_{pit} increases; (b) in simulation predictions. Dashed and continuous lines show trends in data points for different applied pressures. The lines on these figures connect data from the same subsets of the measurement locations and are intended only for visual guidance.

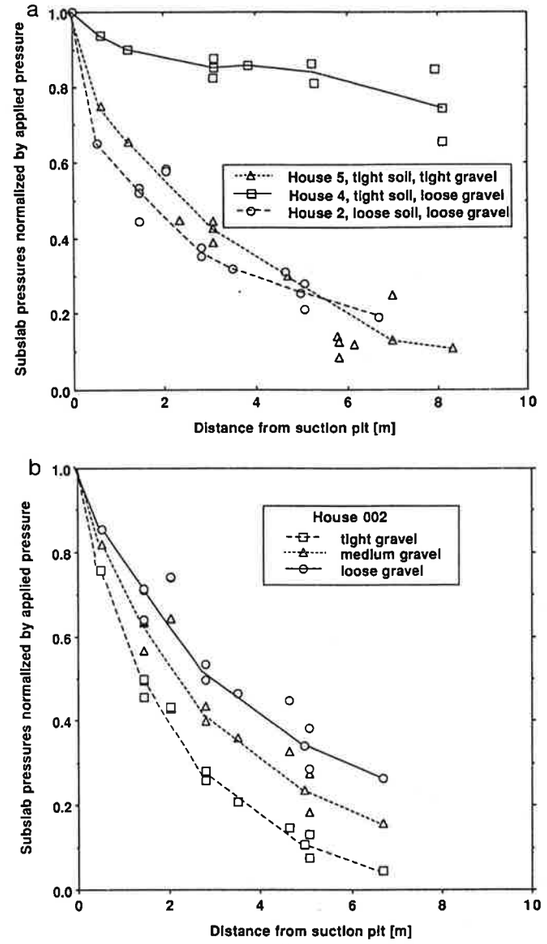

Figure 8. Measured subslab pressure field extension data from three houses with different combinations of soil and aggregate permeability (a) and numerical predictions for house 002 geometry and soil characteristics for three different aggregates (b). See the text for explanation of the terms loose and tight for soils and gravels. Theory predicts that subslab pressure field extension should be excellent when the ratio of aggregate to soil permeability is large, an effect observed in the experimental data shown as well as in the simulation results shown. Since each of the three houses has a different geometry, individual data points should not be directly compared to draw conclusions on panel a. The lines on this figures are intended for visual guidance only.

Effect of Sealing the Cracks. After a first set of field experiments on subslab pressure field extension in house 006, the cracks at the slab/footer joints were carefully sealed, followed by a second set of experiments. Experimental data (Figure 9a) demonstrate the substantial improvement in the subslab pressure field extension following sealing of the cracks. Simulations with the non-Darcy STAR model using the house 002 geometry (note the different house number) also show a similar dramatic improvement in predicted subslab pressure field extension following sealing of all slab/footer cracks (Figure 9b).

Conclusions

A unique field study of SSV system performance was completed in six houses with basements. For each house,

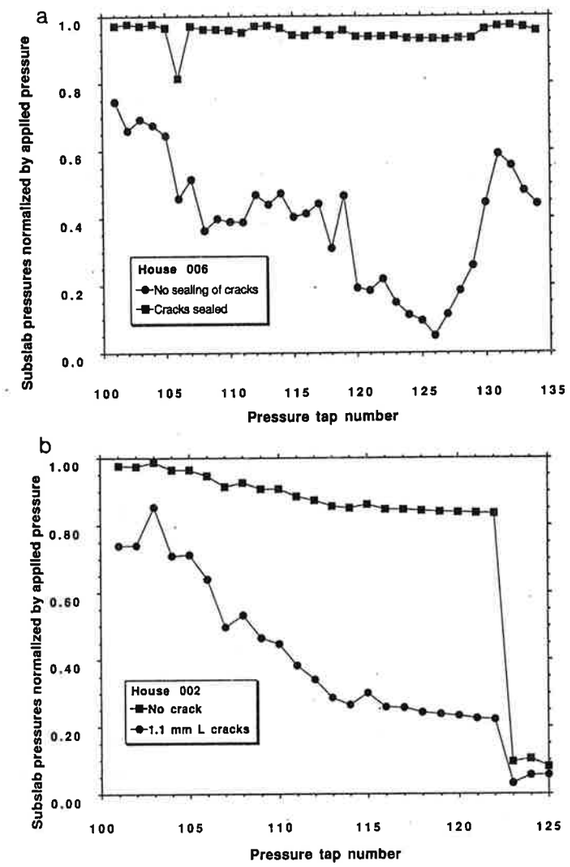

Figure 9. Improvement in the subslab pressure field extension with sealing of slab/footer cracks as demonstrated by experimental data for house 006 (a) and numerical predictions for house 002 (b).

the combination of soil permeability and subslab aggregate permeability was different.

The permeability and Forchheimer factor of samples of three aggregate types used in the field study were measured in the laboratory. Permeability ranged from 2×10^{-8} to 3×10^{-7} m^2, and the Forchheimer factor ranged from 6 to 20 s/m.

A new numerical model of SSV was developed and verified with the field data. The model accounts for non-Darcy flow in the aggregate. Non-Darcy effects were determined to significantly affect SSV performance.

Good extension of the pressure field induced by SSV system operation, throughout the subslab region, is crucial to success of the SSV system in reducing radon entry. For SSD systems, sufficient extension of depressurization in the subslab region prevents convective entry of soil gas into the less depressurized basement. For SSP, we expect that the air flow entering the basement through the cracks will have a low radon concentration, as this air should be primarily fresh air blown in from the SSV pit. However, if the subslab pressure extension due to SSP is not adequate, radon will be advectively transported into depressurized portions of the subslab aggregate layer and then carried into the basement.

Three major conclusions for achieving good extension of the subslab pressure field can be deduced from the trends in field data and numerical predictions: (a) Pressure field extension in the subslab region is very substantially improved if the SSV system is operated with a pit (radius about 25 cm) excavated in the aggregate and soil, at the point where the suction pipe penetrates the basement slab. (b) Sealing all the visible cracks in the slab (including those that appear at the wall/slab joints) to the extent possible leads to a significantly improved performance of SSV system as measured by subslab pressure field extension. (c) When the aggregate is much more permeable than the soil (and cracks and openings in the basement floor are sealed), the aggregate acts as a depressurized manifold with respect to the basement during SSD operation (i.e., there is improved subslab pressure field extension). On the other hand, when the ratio of aggregate permeability to soil permeability is low (specifically, it is smaller than about 2 orders of magnitude), considerable pressure drops can be expected within the aggregate bed.

The verified model provides us with a unique tool for further investigations of SSV system performance. Additional parametric analyses will yield more detailed information for SSV system designers.

Registry No. Rn, 14859-67-7.

Literature Cited

(1) Nero, A. V. *Sci. Am.* **1988**, *258* (5), 42–48.
(2) Nazaroff, W. W.; Nero, A. V. *Radon and its decay products in indoor air*; John Wiley & Sons: New York, 1988.
(3) *EPA Radon reduction techniques for detached houses, technical guidance*, 2nd ed.; EPA/625/5-87/019; U.S. EPA: Washington, DC, 1987.
(4) Washington State Building Code Council. Radon resistive construction standards. *Washington State ventilation and indoor air quality code*; State of Washington: Olympia, WA, 1990; Chapter 5.
(5) Nuess, M. Northwest residential radon standard, Volume 1: project report. Bonneville Power Administration Report; Portland, OR, 1989.
(6) Furman, R. A.; Hintenlang, D. E. Subslab pressure field extension studies on four test slabs typical of Florida Construction. In *Proceedings of the 1990 International Symposium on Radon and Radon Reduction Technology*; Atlanta, GA, Feb 19–23, 1990; EPA/600/9-90/005e; U.S. EPA: Washington, DC, 1990; Vol. V.
(7) Matthews, T. G.; Wilson, D. L.; Terkonda, P. K.; Saultz, R. J.; Goolsby, G.; Burns, S. E.; Haas, J. W. Radon diagnostics: subslab communication and permeability measurements. In *Proceedings of the 1988 International Symposium on Radon and Radon Reduction Technology*; Denver, CO, Oct 17–21, 1988; EPA-600/9-89-006a; U.S. EPA: Washington, DC, 1988; Vol. 1.
(8) Barber, J. M. Mathematical modeling of sub-slab ventilation systems in Florida. M.S Thesis, Nuclear Engineering Sciences, University of FLorida, Gainesville, FL, 1989.
(9) Gadsby, K. J.; Reddy, A. T.; Anderson, D. F.; Gafgen, R.; Craig, A. B. The effect of subslab aggregate size on pressure field extension. In *Proceedings of the 1991 International Symposium on Radon and Radon Reduction Technology*; Philadelphia, PA, Apr 2–5, 1991; U.S. EPA, Washington, DC, 1991, Vol. 4.
(10) Garbesi, K. Experiments and modeling of the soil-gas transport of volatile organic compounds into a residential basement. LBL-25519; Lawrence Berkeley Laboratory: Berkeley, CA, 1988.
(11) Gadgil, A. J.; Bonnefous, Y. C.; Fisk, W. J.; Prill, R. J.; Nematollahi, A. Influence of subslab aggregate permeability on SSV performance. LBL-31160; Lawrence Berkeley Laboratory: Berkeley, CA, 1991.
(12) Loureiro, C. O.; Abriola, L. M.; Martin, J. E.; Sextro, R. G. *Environ. Sci. Technol.* **1990**, *24*, 1338–1348.
(13) Mowris, R. J. Analytical and numerical models for estimating the effects of exhaust ventilation on radon entry in houses with basements or crawl spaces. Report, LBL-22067; Lawrence Berkeley Laboratory: Berkeley CA, 1986.
(14) Revzan, K. L.; Fisk, W. J.; Gadgil, A. J. *Indoor Air* **1991**, *1* (2), 173–189.
(15) Forchheimer, P. H. *Z. Ver. Dtsch. Ing.* **1901**, *45*, 1782–1788.
(16) Patankar, S. V. *Numerical heat transfer and fluid flow*; Hemisphere Publishing: New York, 1980.
(17) Scheidegger, A. E. *The physics of flow through porous media*, 2nd ed.; Macmillan: New York, 1960.

Environ. Sci. Technol. **1992**, *26*, 1759–1764

Received for review February 24, 1992. Revised manuscript received May 14, 1992. Accepted May 15, 1992. This research was supported at Indoor Environment Program of Lawrence Berkeley Laboratory by Bonneville Power Administration (BPA) through Interagency Agreement DE-AI79-90BP06649, and by the Assistant Secretary for Conservation and Renewable Energy, Office of Building Technologies, Building Systems and Materials Division of the U.S. Department of Energy under Contract DE-AC03-76SF00098. This research was also supported at Washington State Energy Office, Energy Extension Service, by BPA Coop Agreement DE-FC79-82BO34623 Modification AO27 (WSE 90-04). Partial support for Y.C.B.'s research participation was granted by ENTPE of Lyon, France.

Diones, Sulfoxides, and Sulfones from the Aerobic Cometabolism of Methylbenzothiophenes by *Pseudomonas* Strain BT1

Sanja Saftić[†] and Phillip M. Fedorak*

Department of Microbiology, University of Alberta, Edmonton, Alberta T6G 2E9, Canada

Jan T. Andersson[‡]

Department of Analytical and Environmental Chemistry, University of Ulm, Postfach 4066, D-7900 Ulm, Germany

■ Six methyl-substituted benzothiophenes were synthesized and used as substrates for *Pseudomonas* strain BT1. These compounds would not support growth but were cometabolized when the culture was grown on 1-methylnaphthalene or glucose. Sulfur-containing metabolites were identified by GC–MS and GC–FTIR and, when possible, by comparison with authentic standards. 2,3-Diones were the metabolites from 4-methylbenzothiophene, 5-methylbenzothiophene, and 6-methylbenzothiophene. Sulfoxides were the major products from 2-methylbenzothiophene and 2,3-dimethylbenzothiophene. Sulfones were also detected as metabolites of the latter two compounds. Cometabolism of 7-methylbenzothiophene yielded the corresponding 2,3-dione, sulfoxide, sulfone, and several other unidentified compounds. Thus, the nature of the metabolites from these methylbenzothiophenes was dependent on the position of the methyl substitution.

Introduction

A wide variety of organosulfur compounds, specifically sulfur heterocycles, are present in many crude oils and coal tars. Their distribution and character depend on the source, maturity, and other alteration processes (*1*). However, although hundreds of the organosulfur compounds have been identified in petroleum, little is known about the implications of their release into the environment (*2*). This is an issue of increasing concern because they are recognized as persistent (*3*, *4*) and potentially harmful environmental pollutants (*5*, *6*). In comparison to the extensive investigations on the microbial metabolism of hydrocarbons and their removal from contaminated environments, little is known about the susceptibility of organosulfur compounds to microbial transformation.

A recent review (*2*) showed that only a small number of known organic sulfur compounds have been used in biotransformation studies because most of the identified compounds are not commercially available. Laboratory experiments with petroleum-degrading bacterial cultures grown on crude oil have shown that the alkylbenzothiophenes were not found in the aromatic fraction of the oils (*7–9*). Similarly, analyses of petroleums that have undergone biodegradation in their reservoirs have shown the absence of alkylbenzothiophenes (*9*, *10*). However, only a few biotransformation products of benzothiophenes have been identified.

There have been several reports on the aerobic cometabolism of benzothiophene (*2*). The transformation products showed oxidation of the thiophene ring at different positions, but no cleavage of either aromatic ring. Benzothiophene and another commercially available compound, 3-methylbenzothiophene (3-MBT), were the focus of a study on the cometabolism of benzothiophenes in the presence of 1-methylnaphthalene (1-MN) (*11*). Cometabolism of benzothiophene yielded benzothiophene-2,3-dione whereas that of 3-methylbenzothiophene yielded predominantly the sulfoxide of 3-methylbenzothiophene with a small amount of the corresponding sulfone.

For this study, six methylbenzothiophenes were synthesized and used as substrates for a pure bacterial culture grown on 1-MN or glucose. The major focus of the study was the identification of the sulfur-containing biotransformation products.

Experimental Section

Chemicals. The methods for synthesis of 2-methylbenzothiophene (2-MBT), 2-methylbenzothiophene *S*,*S*-dioxide (2-MBT sulfone), 5-methylbenzothiophene (5-MBT), 7-methylbenzothiophene (7-MBT), 2,3-dimethylbenzothiophene (2,3-DMBT), and a mixture of 4-methylbenzothiophene (4-MBT) and 6-methylbenzothiophene (6-MBT) are given by Andersson (*12*). 4-MBT was prepared from 2-methylbenzaldehyde (*13*). Sulfones of 7-MBT and 2,3-MBT were synthesized (*14*). 5-Methylbenzothiophene-2,3-dione and 7-methylbenzothiophene-2,3-dione were also synthesized (*15*). *m*-Tolyl methyl sulfoxide and *m*-tolyl methyl sulfone were prepared according to the procedures of Cerniani and Modena (*16*).

Transformations of Methylbenzothiophenes with 1-MN as Growth Substrate. The bacterial strain used for these experiments was isolate BT1, a *Pseudomonas* sp. that can mineralize aromatic hydrocarbons but not aliphatic hydrocarbons (*11*). For each biotransformation study, 10 mL of a BT1 maintenance culture grown on 1-MN was used to inoculate 200 mL of liquid mineral

[†] Present address: Institut für Biotechnologie 3, Forschungszentrum Jülich GmbH, Postfach 1913, 5170 Jülich, Germany.
[‡] Present address: Analytical Chemistry Department, University of Münster, Wilhelm-Klemm-Strasse 8, D-4400 Münster, Germany.

0013-936X/92/0926-1759$03.00/0